Article

Small Electron Polarons in CsPbBr$_3$: Competition between Electron Localization and Delocalization

Nicklas Österbacka, Paul Erhart, Stefano Falletta, Alfredo Pasquarello, and Julia Wiktor*

Cite This: https://dx.doi.org/10.1021/acs.chemmater.0c02345

Read Online

ACCESS | Metrics & More | Article Recommendations

ABSTRACT: We study the nature of excess electrons in CsPbBr$_3$ and identify several single and double polaronic states. We emphasize the importance of proper inclusion of the self-interaction corrections for the stability of small electron polarons in this material. We demonstrate that spin−orbit coupling (SOC) has a significant impact on the energetics of the polaronic states. In particular, we find that SOC disfavors electron localization and leads to different polaronic geometries. Additionally, by carrying out thermodynamic integration, we show that small electron polarons are thermally stabilized in CsPbBr$_3$. The small energy differences between the localized and delocalized electronic states could possibly reconcile the apparently conflicting properties of high charge-carrier mobilities and low recombinations rates.

electrons in CsPbBr$_3$
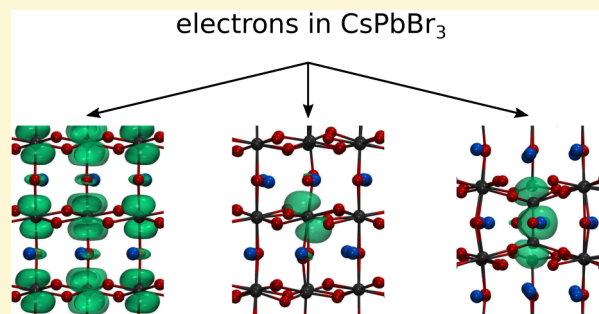
■ INTRODUCTION

Metal halide perovskites have gained remarkable interest as promising materials for optoelectronic applications, for instance, in efficient solar cells.[1−3] The outstanding performance of solar devices based on halide perovskites stems from long lifetimes and diffusion paths of photogenerated electrons and holes,[4−6] among other things. One of the microscale explanations for the low electron−hole recombination rates is based on the formation of polarons.[5,7−12] In particular, it has been shown that the spatial separation between the localized holes and electrons reduces the bimolecular (direct electron−hole) recombination rates,[11] and that the polaron formation suppresses the mononuclear (trap-assisted) recombination processes in CH$_3$NH$_3$PbI$_3$.[12]

Polarons in halide perovskites have already been quite extensively addressed in computational studies.[11−21] However, modeling polarons is not a straightforward task. First, polaron formation in perfect structures at 0 K often requires overcoming a barrier. This means that unless an appropriate initial distortion in the lattice is created, the charge localization will not be found during geometry optimization. Second, to correctly describe localized states, the self-interaction error needs to be addressed. This can be achieved by using a functional that satisfies the generalized Koopmans' theorem. For instance, for the hybrid PBE0(α) functional, this condition can be imposed by tuning the fraction α of Fock exchange. Third, in the case of halide perovskites containing Pb and Sn, the band edges are strongly affected by the relativistic effects resulting from spin−orbit coupling (SOC). It can be expected that SOC also affects the polaronic states. Finally, it was shown

that polarons in CH$_3$NH$_3$PbI$_3$ only form dynamically;[11] therefore, temperature is also expected to affect polaron formation in halide perovskites.

In the present study, we focus on excess electrons in CsPbBr$_3$, which is representative of the larger class of halide perovskites. We show that various single and double polaronic states can be found in this compound. We study how the inclusion of the self-interaction correction affects the binding energies of small electron polarons in CsPbBr$_3$. In particular, we construct a hybrid functional fulfilling Koopmans' condition to overcome the spurious self-interaction. We assess the influence of SOC on the energetics of the polaronic states and demonstrate that the inclusion of SOC can disfavor the electron localization and lead to different polaronic geometries. Finally, by carrying out thermodynamic integration, we show that small electron polarons are thermally stabilized in CsPbBr$_3$.

Computational Details. We perform geometry optimizations and carry out MD simulations using the CP2K package.[22,23] Therein, we employ atom-centered Gaussian-type basis functions to describe the orbitals and an auxiliary plane-wave basis set to re-expand the electron density. DZVP-

MOLOPT basis sets[24] are used. The plane wave basis set is defined up to a cutoff energy of 400 Ha. Core−valence interactions are described by Goedecker−Teter−Hutter pseudopotentials.[25] The calculations at the hybrid functional level are performed using the PBE0(α)[26] functional with the auxiliary density matrix method (ADMM).[27] In the geometry optimization, we sample the Brillouin zone at the Γ-point and neglect the effect of SOC.

To account for SOC, we carry out additional calculations using the Vienna *ab initio* package (VASP).[28,29] In this case, the projector augmented wave method[30] is employed. We use PAW data sets with the following valence orbitals: Cs [5s5p6s], Pb [6s6p], and Br [4s4p]. We set the plane-wave cutoff to 300 eV and sample the Brillouin zone at the Γ-point. We tested the effect of increasing the k-point sampling to $2 \times 2 \times 2$ on the polaron binding energy and found the effect to amount to 0.05 eV only.

Determining the α Parameter. We determine the optimal fraction α of Fock exchange in the PBE0(α) hybrid functional to comply with the generalized Koopmans' theorem in CsPbBr$_3$. In our calculations, we use a $2 \times 2 \times 2$ supercell (160 atoms) of orthorhombic CsPbBr$_3$ with experimental lattice parameters (a = 8.244 Å, b = 11.7351 Å, and c = 8.1982 Å).[31] To identify a localized electronic state, we create an initial distortion by elongating two Pb−Br bonds along the b direction. Then, we carry out a structural relaxation in the presence of one extra electron, using a high fraction of Fock exchange, namely, α = 0.50. This calculation is carried out with the CP2K code (see the Discussion section for more information). In this way, we find an electron polaron localized on one Pb atom, as illustrated in Figure 3a. We remark that two Pb−Br bonds elongate from 3.01 to 3.44 Å. We use this configuration, which is denoted P1, to determine the optimal fraction of exact exchange in a hybrid functional complying with the generalized Koopmans' theorem. We note that, to make sure that the supercell size used in the present study is large enough and that the electron localization is not an artifact, we performed tests in supercells containing up to 1280 atoms. We found the same polaronic configuration in all cells, validating the system size used.

To determine the α parameter in the PBE0 functional, we calculate the single-particle energy level of the electron polaron and of the lowest unoccupied state obtained upon vertical electron extraction. The calculations are done for two different fractions of α, namely, 0.50 and 0.75. We choose two high values of α to ensure that the defect charge remains well localized.[32] To properly determine the single-particle levels, finite-size corrections have to be applied in a careful way. As demonstrated by Falletta et al.,[33] the energy levels need to be corrected in the case of both the initial charged and the final neutral defect state. In the former case, one has to correct the spurious interactions of the polaron with its periodic images and the compensating background charge. In the latter case, even though the cell is neutral, the ionic polarization charge induced by the lattice distortions needs to be accounted for.

To calculate the finite-size corrections, we determine the high-frequency and static dielectric constants ϵ_∞ and ϵ_0 of CsPbBr$_3$. This is done by applying a finite electric field E_j = 0.005 eV/Å in the direction $j \in \{x, y, z\}$.[34,35] We calculate the dielectric tensor ε^{ij} as

$$\varepsilon^{ij} = 1 + \frac{4\pi}{V} \cdot \frac{\Delta P_i}{\Delta E_j} \qquad (1)$$

where V is the cell volume and ΔP_i the response of the polarization in the direction i. We calculate the high-frequency dielectric constant ϵ_∞ by considering only the response of the electrons to the electric field. The static dielectric constant ϵ_0 accounts for both electronic and ionic relaxation. We perform the calculations at two different levels of theory, using semilocal PBE and hybrid PBE0 functionals, respectively. In the latter case, we set the mixing parameter α to 0.50. The calculated values for ϵ_∞ and ϵ_0 are given in Table 1. We remark

Table 1. High-Frequency (ϵ_∞) and Static (ϵ_0) Dielectric Constants of Orthorhombic CsPbBr$_3$

	PBE	PBE0(0.50)
ϵ_∞^{xx}	3.59	3.02
ϵ_∞^{yy}	3.74	3.07
ϵ_∞^{zz}	3.64	3.02
ϵ_0^{xx}	34.95	18.42
ϵ_0^{yy}	29.30	16.51
ϵ_0^{zz}	31.97	16.43

that the dielectric constants for other values of α can be extracted from a linear interpolation of the PBE and PBE0(0.50) results. In the calculation of the finite-size corrections, we use dielectric constants averaged over the x, y, and z directions. We note that the averaged ϵ_∞ calculated at the PBE level (3.66) is in very good agreement with the value measured in recent ellipsometry experiments (3.73).[36]

The dependence of the single-particle energy levels attributed to the electron polaron is shown in Figure 1,
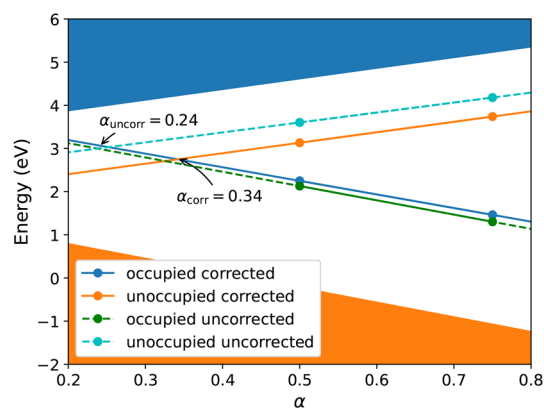

Figure 1. Band edges and single-particle energy levels of the small electron polaron as a function of the fraction of Fock exchange α used in the PBE0(α) calculation. Dashed lines correspond to uncorrected values, while solid lines represent results including finite-size corrections.

including both uncorrected and corrected energy levels. In the latter case, we correct both the occupied and the unoccupied level. For the occupied level, we follow Chen and Pasquarello[37] and apply the following:

$$\epsilon_{corr} = -\frac{2}{q} E_{corr}(q, \varepsilon_0) \qquad (2)$$

to the polaron Kohn−Sham level ϵ_{KS}. In the case of a single small electron polaron, the charge q amounts to -1. $E_{corr}(q, \varepsilon_0)$ corresponds to the finite-size electrostatic correction, which is calculated with the static dielectric constant ε_0 following refs

38 and 39. For the unoccupied level, we follow Falletta et al.[33] In this case, the correction amounts to

$$\epsilon_{corr} = -\frac{2}{q + q'_{pol}} E_{corr}(q + q'_{pol}, \varepsilon_\infty) \tag{3}$$

where q is the charge of the simulation cell, and q'_{pol} is the polarization charge due to the polaronic distortion. $E_{corr}(q + q'_{pol}, \varepsilon_\infty)$ corresponds to the finite-size electrostatic correction calculated for charge $q + q'_{pol}$ with the high-frequency dielectric constant ε_∞. When the finite-size corrections are included, the Koopmans' condition is fulfilled for $\alpha = 0.34$, which is close to the mixing parameter of $\alpha = 0.35$ fulfilling the Koopmans' condition in the case of the bromine vacancy in cubic CsPbBr$_3$.[40] In the following, we use PBE0(0.34) for all determinations of geometries and energies of polaronic configurations. We remark that, by relying on the uncorrected single-particle energy levels, one would obtain $\alpha = 0.22$ for CsPbBr$_3$ for the supercell size considered in the present study (160 atoms). It is thus crucial to take into account finite-size corrections in the determination of the mixing parameter α through Koopmans' condition. This is in agreement with the findings of Kokott et al.[41] in the case of MgO. We note that the α-parameter could also be determined based on other localized states, for instance, related to excess holes. However, we were not able to identify any potentially stable hole polarons in CsPbBr$_3$.

Next, we turn to the calculation of the polaron binding energies. We follow the grand-canonical formulation of defects in crystalline materials[39] and calculate the binding energy E_b as

$$E_b = E_{-1}[pol] - E_0[pristine] - \epsilon_c + E_{corr} \tag{4}$$

where $E_{-1}[pol]$ is the total energy of the relaxed supercell containing the small electron polaron, $E_0[pristine]$ the energy of pristine CsPbBr$_3$, ϵ_c the position of the CBM, and E_{corr} the electrostatic finite-size correction. We note that, in this notation, the negative binding energy indicates that the polaronic state is energetically favorable. For $\alpha = 0.34$, we find that the binding energy of a small electron polaron in orthorhombic CsPbBr$_3$ amounts to -0.24 eV, when neglecting SOC. To highlight the sensitivity of the polaron binding energy to the parametrization of the applied hybrid functional, we show the dependence of E_b on α in Figure 2. As can be observed from the figure, the small electron polaron in CsPbBr$_3$ is not stable for a mixing parameter α lower than about 0.24.

Identifying Polaronic Distortions. Up to now, we focused on one possible polaronic distortion, corresponding to the elongation of the Pb–Br bonds in the b direction. In addition, we demonstrate that polaronic states could arise also for distortions resulting from the elongation of different pairs of Pb–Br bonds. The resulting configurations are shown in Figure 3. We assess the relative stability of these states by calculating their binding energies. The obtained values are reported in Figure 3 and Table 2.

In addition to single electron polarons, we show that bipolarons, consisting of two localized charges, can be formed in CsPbBr$_3$. We find that two electrons can localize on two neighboring Pb atoms, while the bridging Br is pushed toward the center of the cage. We analyze eight distinct bipolaronic configurations, which differ by the Pb pairs on which the electrons are localized and by the directions of the Br displacement. In Figure 4, we show the two most stable
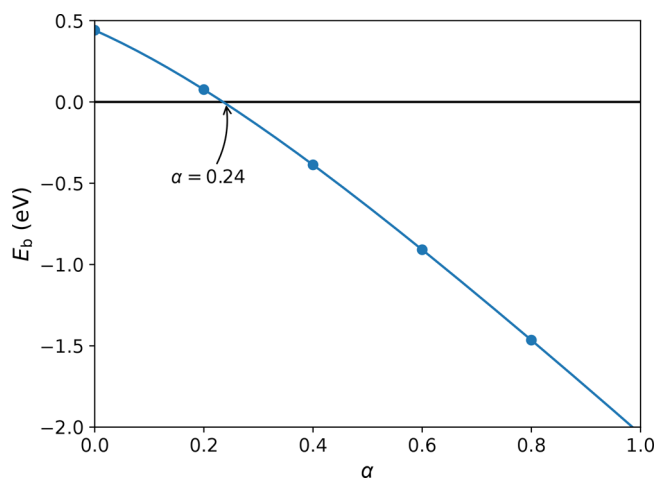

Figure 2. Dependence of the electron polaron binding energy on the fraction of Fock exchange α used in the PBE0(α) calculation.

P1
E_b (w/o SOC) = -0.24 eV
E_b with SOC = $+0.27$ eV

P2
E_b (w/o SOC) = -0.21 eV
E_b with SOC = $+0.28$ eV

P3
E_b (w/o SOC) = -0.26 eV
E_b with SOC = $+0.36$ eV

P4
E_b (w/o SOC) = -0.30 eV
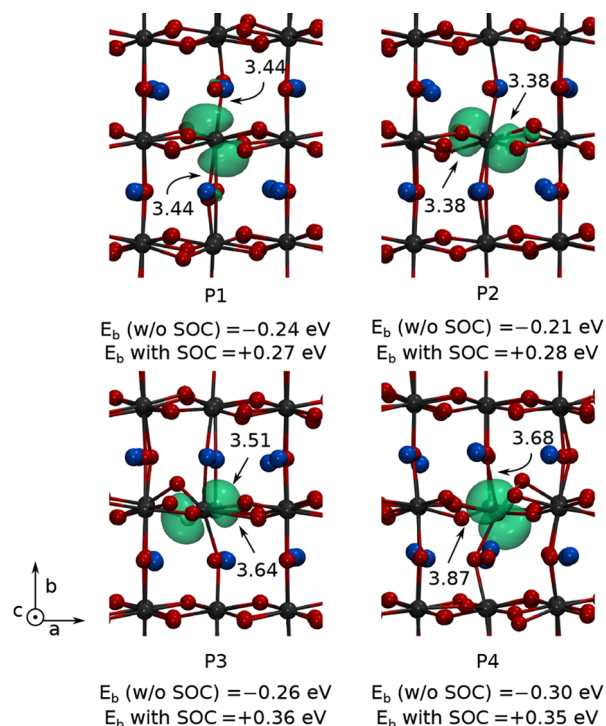E_b with SOC = $+0.35$ eV

Figure 3. Isodensity surfaces (in green) of the electron density associated with electron polaron configurations plotted at 10% of their maximum value. Cs, Pb, and Br atoms are shown in red, gray, and blue, respectively. Binding energies calculated with and without SOC are also given.

bipolaronic configurations. These states have a total spin $S = 0$ and correspond to the formation of Pb–Pb bonds with lengths ranging between 3.23 and 3.24 Å. For the bipolarons, we determine the binding energy per electron, calculated with respect to the delocalized state:

$$E_b = \frac{E_{-2}[bipol] - E_0[pristine] - 2\epsilon_c + E_{corr}}{2} \tag{5}$$

where $E_{-2}[bipol]$ is the total energy of the relaxed supercell containing the bipolaron, and the other quantities are defined as in eq 4. In particular, we find that the total energy of the lowest bipolaronic state is by 1.39 eV lower than that of a

Table 2. Binding Energies of Various Configurations of Single and Double Polarons in CsPbBr$_3$[a]

	$E_b^{withoutSOC}$ (eV)	$E_b^{withSOC}$ (eV)	Δ_{SOC} (eV)
P1	−0.24	0.27	0.52
P2	−0.21	0.28	0.49
P3	−0.26	0.36	0.62
P4	−0.30	0.35	0.65
B1	−0.70	0.09	0.78
B2	−0.68	0.10	0.79

[a]Δ_{SOC} is the difference in the binding energy due to SOC. Polaronic states are labeled as in Figures 3 and 4. We give binding energies per electron to facilitate the comparison between single and double polarons.
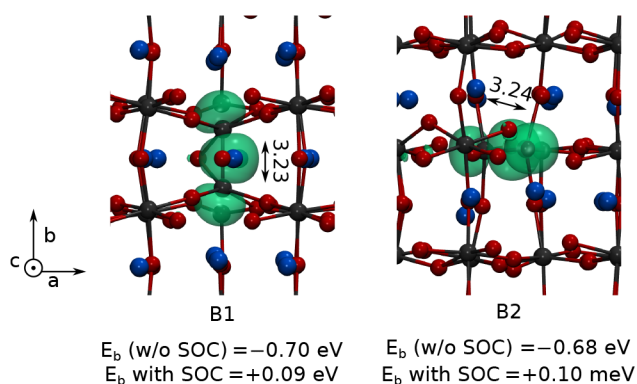

Figure 4. Isodensity surfaces (in green) of the electron density associated with electron bipolaron configurations plotted at 10% of their maximum value. Cs, Pb, and Br atoms are shown in red, gray, and blue, respectively. Binding energies per electron, calculated with and without SOC, are also given.

system with two delocalized electrons. This corresponds to the binding energy of −0.70 eV per electron, significantly lower than the E_b of the single polaron (−0.24 eV).

Effect of SOC. So far, all the calculations were performed without including SOC effects. However, the conduction band edge of halide perovskites, especially of the Pb-based ones, has been shown to be strongly affected by relativistic effects.[42−44] To assess the influence of SOC on polaronic states in CsPbBr$_3$, we perform additional calculations using the Vienna *ab initio* package (VASP)[28,29] on top of the geometries relaxed with CP2K. We note that tests of the computational setup employed within VASP (cutoff energy of 300 eV and Γ-point sampling) showed that the SOC effects on the energy levels of excess electrons are converged within 0.001 eV. We define

$$\Delta^{SOC} = E_b^{withSOC} - E_b^{withoutSOC} \qquad (6)$$

where $E_b^{withSOC}$ and $E_b^{withoutSOC}$ are polaron binding energies calculated with and without SOC included, both calculated within VASP. We then apply Δ_{SOC} to the energies previously obtained with CP2K. To verify the validity of combining results of the two codes, we compare the polaron binding energies in the configurations P1 and B1 without SOC. We find that the energy differs by 0.01 and 0.05 eV only, proving that both codes give a consistent description of the polaronic state. In addition, for these two configurations, we allowed for a further atomic relaxation in VASP and observed no significant changes in the atomic positions, proving that the structures coming from CP2K are reliable.

We evaluate the effect of SOC on the binding energies of the single and double electron polarons in CsPbBr$_3$ (Table 2). We first note that, for all the polaronic configurations, the calculated SOC effect leads to an increase of the binding energies, making the polaronic state unstable. The change in the energy difference between the delocalized and localized electrons depends on how each of these states is affected by SOC. We find that the SOC shifts down in energy, both the CBM and the polaron level. The shift of the CBM amounts to 1.02 eV. On the other hand, the polaron levels show smaller shifts in all cases. For instance, for the electron polaron in the P1 configuration, we find a shift of 0.53 eV. Hence, we conclude that SOC makes the polarons in CsPbBr$_3$ less stable. We remark that the effect on the bipolaronic states is more significant than in the case of single electron polarons. A schematic representation of the effect of SOC on the Kohn−Sham levels corresponding to delocalized and localized levels of the excess electron in CsPbBr$_3$ is given in Figure 5. A similar
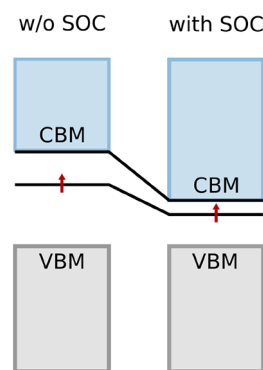

Figure 5. Schematic illustration of the effect of SOC on the Kohn−Sham levels corresponding to delocalized and localized excess electrons in CsPbBr$_3$.

observation about SOC effects making localized charge states less stable was made by Pan et al. in the case of open-shell defects in CdTe.[45] In the case of halide perovskites, it was also shown for the iodine vacancy in CH$_3$NH$_3$PbI$_3$ that SOC disfavors the formation of Pb−Pb dimers.[46]

Furthermore, it should be noted that Δ_{SOC} depends significantly on the geometry of the polaronic state. In particular, for single polarons, the smallest Δ_{SOC} is found for configuration P2 (0.49 eV), which shows the smallest elongations of the Pb−Br bonds. The largest values of Δ_{SOC} are obtained for the bipolaronic state B2 (0.79 eV), which involves the strongest lattice deformation. Therefore, we can conclude that Δ_{SOC} significantly affects the polaronic binding energies and strongly depends on the atomic configuration. This might imply that the polaronic geometries achieved without considering SOC do not reliably represent the energy minima of the localized electrons.

To verify this assumption, we determine the minimum energy path between the configuration of the delocalized electron (pristine supercell) and that of the most stable single polaron state (P1 geometry). This is done by carrying out nudged elastic band (NEB)[47] calculations using CP2K without SOC. Then, we calculate Δ_{SOC} for each configuration using VASP and construct a configuration coordinate diagram including SOC. The results are given in Figure 6, where we also show the dependence of Δ_{SOC} on the bond elongation. We observe that the dependence of the total energy on the lattice
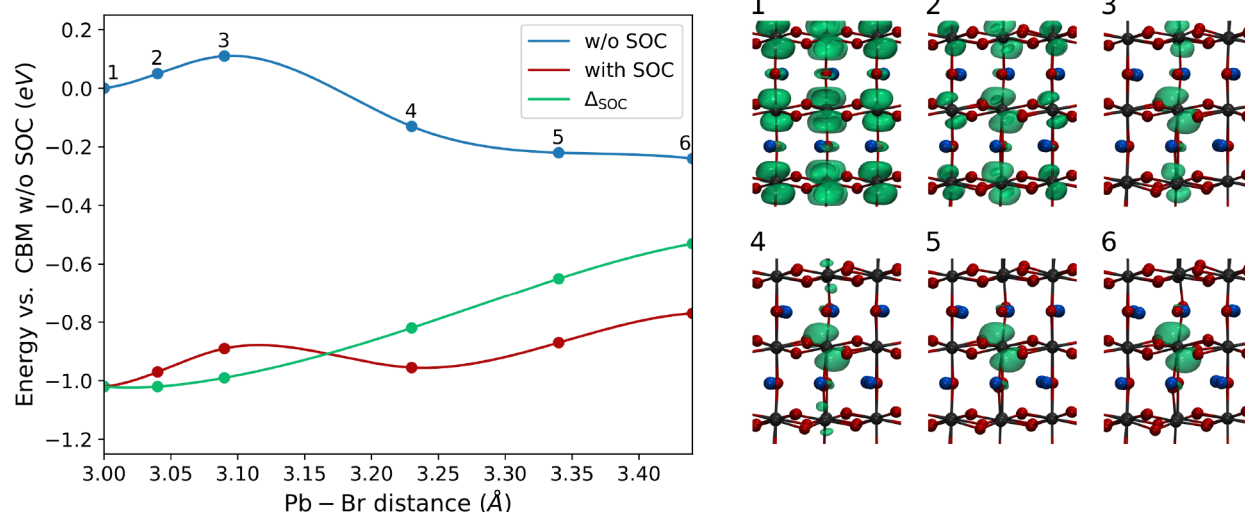
Figure 6. Dependence of the total energy of a CsPbBr$_3$ cell containing one excess electron as a function of Pb−Br distance, with and without the SOC contribution. The values are given with respect to the pristine cell. Δ_{SOC} represents the energy difference between the cases with and without SOC. The isodensity surface of the extra electron is shown in green for each geometry.

deformation, represented here by the longest Pb−Br bond in the configuration, is affected by SOC. For bond lengths between 3.08 and 3.44 Å, we find an almost linear dependence between Δ_{SOC} and the Pb−Br distance. As a result, the geometry achieved by relaxing the polaron while neglecting SOC no longer corresponds to a minimum in energy once SOC is included. The minimum along the considered path is now found when the Pb−Br bond is elongated to about 3.22 Å only. This polaronic configuration is still higher in energy than the delocalized electronic state. However, the energy difference amounts to only 0.07 eV, once SOC is included.

Thermal Effects on Polaron Formation. It has been demonstrated previously for CH$_3$NH$_3$PbI$_3$[11,18] and BiVO$_4$[48,49] that the stability of small polarons can be affected by thermal effects. It is especially important to assess the thermal effects on the polaronic state in CsPbBr$_3$, considering that there is only a small energy difference between the delocalized and localized electronic states at 0 K. To calculate the binding energy of the small polaron at 300 K, we replace the total energies E in eq 4 with free energies G:

$$E_b = G_{-1}[pol] - G_0[pristine] + \epsilon_c + E_{corr} \tag{7}$$

where $G_{-1}[pol]$ is the free energy of the localized electron, and $G_0[pristine]$ is that of the pristine material. To calculate the free energy difference $G_{-1}[pol] - G_0[pristine]$ at room temperature, we use the thermodynamic integration (TI) method.[50] We introduce a fictitious Hamiltonian $\mathcal{H}_\eta$:

$$\mathcal{H}_\eta = \eta\mathcal{H}[pol] + (1 - \eta)\mathcal{H}[pristine] \tag{8}$$

which connects the Hamiltonian of the pristine material with that of the electron polaron, through the Kirkwood coupling parameter η. In this case, η represents the fraction of the electron that is included in the cell. The relevant free energy difference is then calculated as

$$G_{-1}[pol] - G_0[pristine] = \int_0^1 \langle\Delta E\rangle_\eta \, d\eta \tag{9}$$

where $\langle\Delta E\rangle_\eta$ is the vertical energy of the electron averaged over the MD trajectory generated with the corresponding value of η. The TI is based on an MD run of about 5 ps, with a time

step of 5 fs. We only include the last 3 ps in the statistics. In the TI, we use CP2K and neglect SOC effects, since their inclusion in hybrid functional MD simulations is computationally prohibitive. The integration is done using six values of η, namely, 0.0, 0.5, 0.7, 0.8, 0.9, and 1.0. We initiate the simulations with nonzero charge and the P1 polaronic configuration. The relationship between $\langle\Delta E\rangle_\eta$ and η is given in Figure 7. For η lower than 0.7, there is no significant
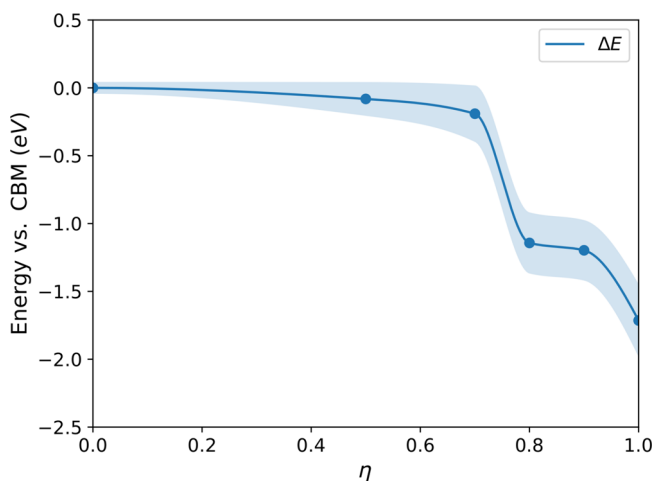

Figure 7. Vertical electron extraction energy averaged over MD trajectories achieved with the corresponding values of η. The shaded area represents the standard deviation. Energies are given with respect to the average position of the CBM of the neutral cell.

localization, and the vertical extraction energy corresponds to the position of the CBM. In the simulations with η between 0.8 and 1.0, a small electron polaron is formed, and a deep occupied level appears inside the band gap. We observe significant fluctuations in this level, as shown by standard deviations ranging up to 0.27 eV in Figure 7. Using eq 7, we find that the binding energy of the small electron polaron is about −0.45 eV. This means that the polaronic state is thermally stabilized by about 0.21 eV. This shift of the

polaronic level toward lower energies is close to what was calculated for an electron polaron in $BiVO_4$ (0.16 eV on the absolute energy scale).[48] We assume that the energy reduction due to finite temperature can also be applied to the polaronic binding energy calculated accounting for SOC. This is justified on the basis that the polaron binding energy can be separated into two parts. The first one is related to the strain required to distort the lattice. The second stems from the electronic energy gained by localizing the electron.[51] The finite temperature makes the polaron more stable by reducing the cost of lattice deformations, while maintaining the electronic part mostly unaffected. The SOC, on the other hand, mostly affects the electronic part of the energy. Therefore, the two effects are expected to be largely independent. By combining the thermal stabilization (−0.21 eV) with the E_b calculated with SOC (0.07 eV), we derive a polaron binding energy of −0.14 eV at 300 K. We also expect that thermal effects could lead to negative binding energies of the bipolaronic states B1 (E_b = 0.09 eV at 0 K) and B2 (E_b = 0.10 eV at 0 K). However, due to the differences in the local geometries, the thermal stabilization calculated for the single polaron cannot be trivially applied to these configurations.

■ DISCUSSION

We note that the formation energies of the polaronic state found in the present study are quite small. We estimate that electron localization in the single polaronic states is favored by about 0.1 eV per electron at room temperature. This is likely close to the accuracy of our computational setup. Nevertheless, qualitative conclusions can be drawn from these results.

We have shown that the energy landscape of an extra electron in $CsPbBr_3$ is rather flat. The Pb−Br bonds can be stretched quite easily in the charged system, as shown in Figure 6. This can imply that electrons at finite temperature can exhibit a dual nature, with a dynamical competition between localized and delocalized states. This is further enhanced by large fluctuations of the single-particle energy level corresponding to the electron polaron, described by standard deviations ranging up to 0.27 eV (see Figure 7).

First, we note that the dual behavior of excess electrons in $CsPbBr_3$ could contribute to the explanation of the high performance of photovoltaic devices based on halide perovskites. It has been previously shown that polaron formation can reduce charge recombination,[11,12,52] thereby increasing the lifetimes of the photogenerated charges. However, the formation of small polarons is often related to a significant reduction in charge-carrier mobility.[53−55] For instance, in $BiVO_4$, the formation of small electron polarons leads to extremely low carrier mobilities ($\approx 10^{-2}$ cm^2 V^{-1} s^{-1}).[54] For halide perovskites, much higher mobilities have been observed. For instance, an electron mobility of 66 cm^2 V^{-1} s^{-1} was reported for $CH_3NH_3PbI_3$ in ref 56. Our results indicate that the delocalized and localized electronic states are close in energy in $CsPbBr_3$ and should coexist in the material. Therefore, the excess electrons can exhibit relatively high mobilities while being protected from recombination by strong spatial localization.

Second, the dual nature of extra electrons in $CsPbBr_3$ can partially explain the conflicting observations made for charge-carrier mobilities themselves. Generally, it was observed that charge-carrier mobilities in halide perovskites are rather well described within the Fröhlich model,[13,57] in which a weakly localized charge moves through the material while interacting with the lattice. However, e.g., for $CH_3NH_3PbI_3$, the Fröhlich model predicts that the charge mobility μ should depend on temperature through $\mu \propto T^{-0.46}$, while the measurements indicate a $\mu \propto T^{-1.5}$ relationship.[57] This implies that there is another mechanism that limits the charge-carrier mobility in halide perovskites. We propose that the dynamic small polaron formation also affects the total mobility. As noted by Herz in ref 57, the experimental data are relatively noisy and could correspond to a wider distribution of exponents. The coexistence of polarons and delocalized electrons in halide perovskites, supported by our calculations, would imply at least two contributions to the mobility with presumably different temperature dependences.

■ CONCLUSIONS

In conclusion, we studied electron localization in $CsPbBr_3$. We first demonstrated the importance of the proper inclusion of the self-interaction correction in evaluating the energetics of localized electrons. We determined the hybrid functional parameter fulfilling Koopmans' condition, while accounting for finite-size errors in the polaronic level. Second, we showed that electron polarons in $CsPbBr_3$ can form in several geometries, in the case of both single and double charge localization. We further observed that SOC makes polarons less stable relative to the delocalized electronic state. We showed that the effect of SOC corresponds to a complex interplay between the shifts in the CBM and the polaronic level. In addition, the effect of SOC on the polaronic level depends on the atomic arrangement and shifts the minima in the potential energy surface. We finally studied the thermal effects on the small polaron in $CsPbBr_3$ through thermodynamic integration at 300 K. We showed that thermal effects enhance the stabilization of the polaronic state by about 0.21 eV thereby counteracting the destabilization effect due to SOC. From our results, we thus infer that the polaron state is more stable than the delocalized electron by about 0.1 eV. Our results suggest that at finite temperatures, electrons in $CsPbBr_3$ can exhibit a dual behavior, in which the strong spatial localization, which protects them from recombination, competes with delocalization allowing for relatively high mobilities.

■ AUTHOR INFORMATION

Corresponding Author

Julia Wiktor − *Department of Physics, Chalmers University of Technology, SE-412 96 Gothenburg, Sweden;* ● orcid.org/0000-0003-3395-1104; Email: julia.wiktor@chalmers.se

Authors

Nicklas Österbacka − *Department of Physics, Chalmers University of Technology, SE-412 96 Gothenburg, Sweden;* ● orcid.org/0000-0002-6043-4607

Paul Erhart − *Department of Physics, Chalmers University of Technology, SE-412 96 Gothenburg, Sweden;* ● orcid.org/0000-0002-2516-6061

Stefano Falletta − *Chaire de Simulation à l'Echelle Atomique (CSEA), Ecole Polytechnique Fédérale de Lausanne (EPFL), CH-1015 Lausanne, Switzerland;* ● orcid.org/0000-0003-3971-5911

Alfredo Pasquarello − *Chaire de Simulation à l'Echelle Atomique (CSEA), Ecole Polytechnique Fédérale de Lausanne (EPFL), CH-1015 Lausanne, Switzerland;* ● orcid.org/0000-0002-9142-2799

Complete contact information is available at:

https://pubs.acs.org/10.1021/acs.chemmater.0c02345

Notes

■ ACKNOWLEDGMENTS

■ REFERENCES

(1) Kojima, A.; Teshima, K.; Shirai, Y.; Miyasaka, T. Organometal Halide Perovskites as Visible-Light Sensitizers for Photovoltaic Cells. *J. Am. Chem. Soc.* **2009**, *131*, 6050−6051.

(2) Hodes, G. Perovskite-Based Solar Cells. *Science* **2013**, *342*, 317−318.

(3) Green, M. A.; Ho-Baillie, A.; Snaith, H. J. The Emergence of Perovskite Solar Cells. *Nat. Photonics* **2014**, *8*, 506.

(4) Stranks, S. D.; Eperon, G. E.; Grancini, G.; Menelaou, C.; Alcocer, M. J.; Leijtens, T.; Herz, L. M.; Petrozza, A.; Snaith, H. J. Electron-Hole Diffusion Lengths Exceeding 1 Micrometer in an Organometal Trihalide Perovskite Absorber. *Science* **2013**, *342*, 341−344.

(5) Wehrenfennig, C.; Eperon, G. E.; Johnston, M. B.; Snaith, H. J.; Herz, L. M. High Charge Carrier Mobilities and Lifetimes in Organolead Trihalide Perovskites. *Adv. Mater.* **2014**, *26*, 1584−1589.

(6) Bi, Y.; Hutter, E. M.; Fang, Y.; Dong, Q.; Huang, J.; Savenije, T. J. Charge Carrier Lifetimes Exceeding 15 μs in Methylammonium Lead Iodide Single Crystals. *J. Phys. Chem. Lett.* **2016**, *7*, 923−928.

(7) Chen, Y.; Yi, H.; Wu, X.; Haroldson, R.; Gartstein, Y.; Rodionov, Y.; Tikhonov, K.; Zakhidov, A.; Zhu, X.-Y.; Podzorov, V. Extended Carrier Lifetimes and Diffusion in Hybrid Perovskites Revealed by Hall Effect and Photoconductivity Measurements. *Nat. Commun.* **2016**, *7*, 12253.

(8) Johnston, M. B.; Herz, L. M. Hybrid Perovskites for Photovoltaics: Charge-Carrier Recombination, Diffusion, and Radiative Efficiencies. *Acc. Chem. Res.* **2016**, *49*, 146−154.

(9) Bokdam, M.; Sander, T.; Stroppa, A.; Picozzi, S.; Sarma, D.; Franchini, C.; Kresse, G. Role of Polar Phonons in the Photo Excited State of Metal Halide Perovskites. *Sci. Rep.* **2016**, *6*, 28618.

(10) Zhu, H.; Miyata, K.; Fu, Y.; Wang, J.; Joshi, P. P.; Niesner, D.; Williams, K. W.; Jin, S.; Zhu, X.-Y. Screening in Crystalline Liquids Protects Energetic Carriers in Hybrid Perovskites. *Science* **2016**, *353*, 1409−1413.

(11) Ambrosio, F.; Wiktor, J.; De Angelis, F.; Pasquarello, A. Origin of Low Electron−Hole Recombination Rate in Metal Halide Perovskites. *Energy Environ. Sci.* **2018**, *11*, 101−105.

(12) Wiktor, J.; Ambrosio, F.; Pasquarello, A. Mechanism Suppressing Charge Recombination at Iodine Defects in $CH_3NH_3PbI_3$ by Polaron Formation. *J. Mater. Chem. A* **2018**, *6*, 16863−16867.

(13) Frost, J. M. Calculating Polaron Mobility in Halide Perovskites. *Phys. Rev. B: Condens. Matter Mater. Phys.* **2017**, *96*, 195202.

(14) Peng, C.; Wang, J.; Wang, H.; Hu, P. Unique Trapped Dimer State of the Photogenerated Hole in Hybrid Orthorhombic $CH_3NH_3PbI_3$ Perovskite: Identification, Origin, and Implications. *Nano Lett.* **2017**, *17*, 7724−7730.

(15) Neukirch, A. J.; Abate, I. I.; Zhou, L.; Nie, W.; Tsai, H.; Pedesseau, L.; Even, J.; Crochet, J. J.; Mohite, A. D.; Katan, C.; Tretiak, S. Geometry Distortion and Small Polaron Binding Energy Changes with Ionic Substitution in Halide Perovskites. *J. Phys. Chem. Lett.* **2018**, *9*, 7130−7136.

(16) Kang, B.; Biswas, K. Exploring Polaronic, Excitonic Structures and Luminescence in Cs_4PbBr_6/$CsPbBr_3$. *J. Phys. Chem. Lett.* **2018**, *9*, 830−836.

(17) Mahata, A.; Meggiolaro, D.; De Angelis, F. From Large to Small Polarons in Lead, Tin, and Mixed Lead−Tin Halide Perovskites. *J. Phys. Chem. Lett.* **2019**, *10*, 1790−1798.

(18) Ambrosio, F.; Meggiolaro, D.; Mosconi, E.; De Angelis, F. Charge Localization, Stabilization, and Hopping in Lead Halide Perovskites: Competition Between Polaron Stabilization and Cation Disorder. *ACS Energy Lett.* **2019**, *4*, 2013−2020.

(19) Ambrosio, F.; Meggiolaro, D.; Mosconi, E.; De Angelis, F. Charge Localization and Trapping at Surfaces in Lead-Iodide Perovskites: The Role of Polarons and Defects. *J. Mater. Chem. A* **2020**, *8*, 6882−6892.

(20) Meggiolaro, D.; Ambrosio, F.; Mosconi, E.; Mahata, A.; De Angelis, F. Polarons in Metal Halide Perovskites. *Adv. Energy Mater.* **2020**, *10*, 1902748.

(21) Wolf, M. J.; Irvine, L. A. D.; Walker, A. B. Quantifying Polaronic Effects on Charge-Carrier Scattering and Mobility in Lead−Halide Perovskites. *arXiv.org*, 2020, arXiv:2003.00968. https://arxiv.org/abs/2003.00968 (accessed 2020-09-23).

(22) VandeVondele, J.; Krack, M.; Mohamed, F.; Parrinello, M.; Chassaing, T.; Hutter, J. Quickstep: Fast and Accurate Density Functional Calculations Using a Mixed Gaussian and Plane Waves Approach. *Comput. Phys. Commun.* **2005**, *167*, 103−128.

(23) Kühne, T. D.; et al. CP2K: An Electronic Structure and Molecular Dynamics Software Package-Quickstep: Efficient and Accurate Electronic Structure Calculations. *J. Chem. Phys.* **2020**, *152*, 194103.

(24) VandeVondele, J.; Hutter, J. Gaussian Basis Sets for Accurate Calculations on Molecular Systems in Gas and Condensed Phases. *J. Chem. Phys.* **2007**, *127*, 114105.

(25) Goedecker, S.; Teter, M.; Hutter, J. Separable Dual-Space Gaussian Pseudopotentials. *Phys. Rev. B: Condens. Matter Mater. Phys.* **1996**, *54*, 1703.

(26) Perdew, J. P.; Ernzerhof, M.; Burke, K. Rationale for Mixing Exact Exchange with Density Functional Approximations. *J. Chem. Phys.* **1996**, *105*, 9982−9985.

(27) Guidon, M.; Hutter, J.; VandeVondele, J. Auxiliary Density Matrix Methods for Hartree- Fock Exchange Calculations. *J. Chem. Theory Comput.* **2010**, *6*, 2348−2364.

(28) Kresse, G.; Hafner, J. Ab Initio Molecular Dynamics for Liquid Metals. *Phys. Rev. B: Condens. Matter Mater. Phys.* **1993**, *47*, 558.

(29) Kresse, G.; Furthmüller, J. Efficient Iterative Schemes for Ab Initio Total-Energy Calculations Using a Plane-Wave Basis Set. *Phys. Rev. B: Condens. Matter Mater. Phys.* **1996**, *54*, 11169.

(30) Blöchl, P. E. Projector Augmented-Wave Method. *Phys. Rev. B: Condens. Matter Mater. Phys.* **1994**, *50*, 17953.

(31) Stoumpos, C. C.; Malliakas, C. D.; Peters, J. A.; Liu, Z.; Sebastian, M.; Im, J.; Chasapis, T. C.; Wibowo, A. C.; Chung, D. Y.; Freeman, A. J.; Wessels, B. W.; Kanatzidis, M. G. Crystal Growth of the Perovskite Semiconductor $CsPbBr_3$: A New Material for High-Energy Radiation Detection. *Cryst. Growth Des.* **2013**, *13*, 2722−2727.

(32) Miceli, G.; Chen, W.; Reshetnyak, I.; Pasquarello, A. Nonempirical Hybrid Functionals for Band Gaps and Polaronic Distortions in Solids. *Phys. Rev. B: Condens. Matter Mater. Phys.* **2018**, *97*, 121112.

(33) Falletta, S.; Wiktor, J.; Pasquarello, A. Finite-Size Corrections of Defect Energy Levels Involving Ionic Polarization. *Phys. Rev. B: Condens. Matter Mater. Phys.* **2020**, *102*, 041115.

(34) Umari, P.; Pasquarello, A. Ab Initio Molecular Dynamics in a Finite Homogeneous Electric Field. *Phys. Rev. Lett.* **2002**, *89*, 157602.

(35) Souza, I.; Íñiguez, J.; Vanderbilt, D. First-Principles Approach to Insulators in Finite Electric Fields. *Phys. Rev. Lett.* **2002**, *89*, 117602.

(36) Chen, X.; Wang, Y.; Song, J.; Li, X.; Xu, J.; Zeng, H.; Sun, H. Temperature Dependent Reflectance and Ellipsometry Studies on a CsPbBr3 Single Crystal. *J. Phys. Chem. C* **2019**, *123*, 10564−10570.

(37) Chen, W.; Pasquarello, A. Correspondence of Defect Energy Levels in Hybrid Density Functional Theory and Many-Body Perturbation Theory. *Phys. Rev. B: Condens. Matter Mater. Phys.* **2013**, *88*, 115104.

(38) Komsa, H.-P.; Rantala, T. T.; Pasquarello, A. Finite-Size Supercell Correction Schemes for Charged Defect Calculations. *Phys. Rev. B: Condens. Matter Mater. Phys.* **2012**, *86*, 045112.

(39) Freysoldt, C.; Grabowski, B.; Hickel, T.; Neugebauer, J.; Kresse, G.; Janotti, A.; Van de Walle, C. G. First-Principles Calculations for Point Defects in Solids. *Rev. Mod. Phys.* **2014**, *86*, 253−305.

(40) Bischoff, T.; Wiktor, J.; Chen, W.; Pasquarello, A. Nonempirical Hybrid Functionals for Band Gaps of Inorganic Metal-Halide Perovskites. *Phys. Rev. Mater.* **2019**, *3*, 123802.

(41) Kokott, S.; Levchenko, S. V.; Rinke, P.; Scheffler, M. First-Principles Supercell Calculations of Small Polarons with Proper Account for Long-Range Polarization Effects. *New J. Phys.* **2018**, *20*, 033023.

(42) Menéndez-Proupin, E.; Palacios, P.; Wahnón, P.; Conesa, J. Self-Consistent Relativistic Band Structure of the $CH_3NH_3PbI_3$ Perovskite. *Phys. Rev. B: Condens. Matter Mater. Phys.* **2014**, *90*, 045207.

(43) Brivio, F.; Butler, K. T.; Walsh, A.; Van Schilfgaarde, M. Relativistic Quasiparticle Self-Consistent Electronic Structure of Hybrid Halide Perovskite Photovoltaic Absorbers. *Phys. Rev. B: Condens. Matter Mater. Phys.* **2014**, *89*, 155204.

(44) Wiktor, J.; Rothlisberger, U.; Pasquarello, A. Predictive Determination of Band Gaps of Inorganic Halide Perovskites. *J. Phys. Chem. Lett.* **2017**, *8*, 5507−5512.

(45) Pan, J.; Metzger, W. K.; Lany, S. Spin-Orbit Coupling Effects on Predicting Defect Properties with Hybrid Functionals: A Case Study in CdTe. *Phys. Rev. B: Condens. Matter Mater. Phys.* **2018**, *98*, 054108.

(46) Meggiolaro, D.; De Angelis, F. First-Principles Modeling of Defects in Lead Halide Perovskites: Best Practices and Open Issues. *ACS Energy Lett.* **2018**, *3*, 2206−2222.

(47) Henkelman, G.; Jónsson, H. Improved Tangent Estimate in the Nudged Elastic Band Method for Finding Minimum Energy Paths and Saddle Points. *J. Chem. Phys.* **2000**, *113*, 9978−9985.

(48) Wiktor, J.; Ambrosio, F.; Pasquarello, A. Role of Polarons in Water Splitting: The Case of $BiVO_4$. *ACS Energy Lett.* **2018**, *3*, 1693−1697.

(49) Wiktor, J.; Pasquarello, A. Electron and Hole Polarons at the $BiVO_4$-Water Interface. *ACS Appl. Mater. Interfaces* **2019**, *11*, 18423−18426.

(50) Frenkel, D.; Smit, B. *Understanding Molecular Simulation: From Algorithms to Applications*; Academic Press: San Diego, CA, 2002.

(51) Janotti, A.; Franchini, C.; Varley, J.; Kresse, G.; Van de Walle, C. Dual Behavior of Excess Electrons in Rutile TiO_2. *Phys. Status Solidi RRL* **2013**, *7*, 199−203.

(52) Zhou, F.; Sadigh, B.; Erhart, P.; Åberg, D. Ab Initio Prediction of Fast Non-Equilibrium Transport of Nascent Polarons in SrI_2: A Key to High-Performance Scintillation. *npj Comput. Mater.* **2016**, *2*, 1−7.

(53) Plata, J. J.; Marquez, A. M.; Sanz, J. F. Electron Mobility Via Polaron Hopping in Bulk Ceria: A First-Principles Study. *J. Phys. Chem. C* **2013**, *117*, 14502−14509.

(54) Butler, K.; Dringoli, B.; Zhou, L.; Rao, P.; Walsh, A.; Titova, L. Ultrafast Carrier Dynamics in $BiVO_4$ Thin Film Photoanode Material: Interplay Between Free Carriers, Trapped Carriers and Low-Frequency Lattice Vibrations. *J. Mater. Chem. A* **2016**, *4*, 18516−18523.

(55) Wu, F.; Ping, Y. Combining Landau−Zener Theory and Kinetic Monte Carlo Sampling for Small Polaron Mobility of Doped $BiVO_4$ from First-Principles. *J. Mater. Chem. A* **2018**, *6*, 20025−20036.

(56) Stoumpos, C. C.; Malliakas, C. D.; Kanatzidis, M. G. Semiconducting Tin and Lead Iodide Perovskites with Organic Cations: Phase Transitions, High Mobilities, and Near-Infrared Photoluminescent Properties. *Inorg. Chem.* **2013**, *52*, 9019−9038.

(57) Herz, L. M. How Lattice Dynamics Moderate the Electronic Properties of Metal-Halide Perovskites. *J. Phys. Chem. Lett.* **2018**, *9*, 6853−6863.